MODELING OF THE MOVING INDUCTION HEATING USED IN WELD-BASED ADDTIVE MANUFACTURING

X. W. Bai*, H. O Zhang*†, and G. L. Wang**

* State Key Laboratory of Digital Manufacturing Equipment and Technology, Huazhong University of Science and Technology, Wuhan 430074, PR China
** State Key Laboratory of Materials Processing and Die & Mould Technology, Huazhong University of Science and Technology, Wuhan 430074, PR China

Abstract

This paper numerically investigates the application induction heating in weld-based additive manufacturing to reduce residual stresses. To avoid time-consuming transient electromagnetic calculation, the induction heat is assumed to be constant in the arc coordinate. Thermo-electromagnetic coupling analysis is performed only at a typical time to obtain the representative distribution of induction heat, which is then transferred to the thermal analysis of multilayer deposition as a secondary heat source. Furthermore, the effects of real-time induction preheating and postheating on residual stress state are analyzed in comparative simulations. The results show that both induction preheating and postheating lead to more homogeneous heat input and lower residual stresses compared with the case without induction heating.

Introduction

An effective approach to recduce residual stresses in Weld-based Additive Manufacturing (WAM) is to make additional thermal intervention during or after fabrication through induction heating or other means. In the so-called induction heating assisted WAM, controllable induction heat is quickly generated in precisely located area of the deposited component at specified time, which greatly facilitates the process to obtain required thermal field that produces smaller stresses. Actually, induction heating has been widely used to reduce residual stresses and cracks in welding [1] and additive manufacturing processes [2].

By far, several researches have been devoted to the thermo-mechanical modeling of WAM process. Mughal et al. [3] predicted the stress-induced deformations in WAM using a three-dimensional finite element model. Three-dimensional thermal analysis [4] and mechanical analysis [5] conducted by Zhao et al. reported that the deposition in reverse directions results in improved heat diffusion condition and lower stresses. Ding et al. [6] employed thermo-elastic-plastic FEM to simulate the thermo-mechanical performance of large multi-layer wall-shaped structure fabricated by wire and arc additive manufacturing. Based on the discovery that the peak temperature experienced during thermal cycles in deposition determine the residual stress of that point, Ding et al. [7] also developed an engineering FE model to predict distortion and residual stress more efficiently and reported a computational time save by 99%. Bai et al. [8] improved the prediction accuracy of thermal analysis for WAM by calibrating input parameters using infrared (IR) imaging. However, there are no studies on the simulation of WAM process with additional induction heating.

The simulation of induction-assisted WAM is a tough task because arc and induction heat work simultaneously and interact mutually during deposition; a transient thermo-electromagnetic coupling analysis over long deposition time according to conventional simulation strategy would result in unaffordable computational cost. Thus, a simplification strategy is desirable for simulation. This paper presents a new numerical strategy which models the induction heat as a secondary heat source besides the arc. The simulation

of induction-assisted WAM process is realized at reasonable computational cost by avoiding the coupling analysis at each time step. Furthermore, the effects of real-time induction preheating and postheating on residual stress state are investigated through comparative simulations.

Experimental

As shown in Figure 1, thin-wall components were deposited using WAM on the side edge of previously stress-relieved base plates. AWS ER70S-6 mild steel wire was employed as the welding consumables. The material deposition and the movements of arc torch and inductor were controlled by a Motoman robot. After depositions, the residual stresses were measured using X-ray diffraction (XRD) method.
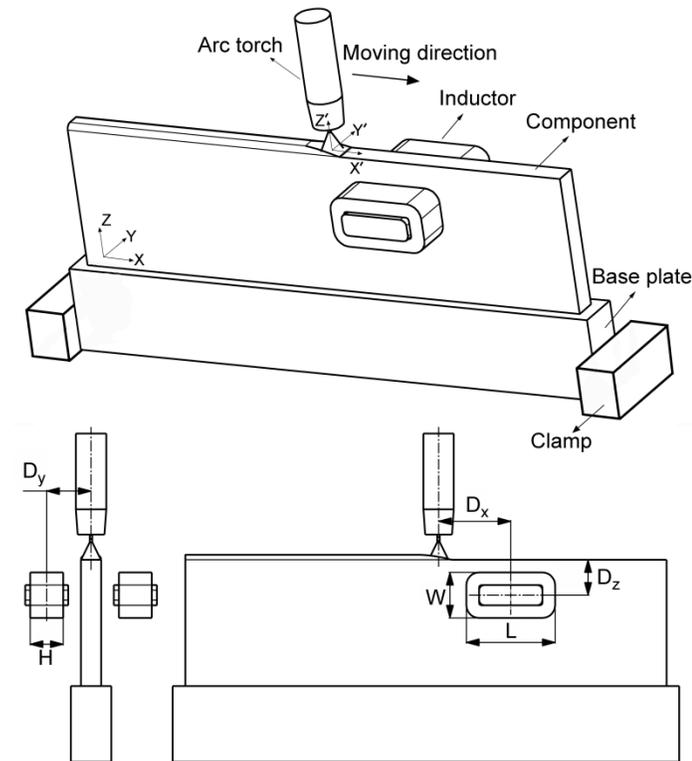

Figure 1: Experimental setup

The inductor consists of two symmetrical coils mounted on both sides of the workpiece. This design approximates to the transverse flux induct heating (TFIH). The role of induction heating differs with the position of inductor. The inductor performs real-time preheating if moving ahead of the arc, or real-time postheating behind the arc. As shown in Figure 1, two coordinate systems, namely the fixed workpiece coordinate (X, Y, Z) and the moving arc coordinate (X', Y', Z'), were established for convenient mathematic description. L, W and H refer to the size of the inductor; D_x, D_y and D_z illustrate the relative distances between the inductor and the arc.

Numerical models and simulation procedure

1. Simulation procedure

As mentioned above, simplification must be made for this transient thermo-electromagnetic coupling problem. During deposition, the inductor is moving with the arc torch, producing an induction heating zone

generally much smaller than the workpiece. Under this circumstance, it is an acceptable assumption that induction heat generation remains a constant distribution in the moving arc coordinate during deposition, then the induction heat generation distribution obtained by a coupling analysis at a typical moment during deposition could be used to represent the situations in all cases and be loaded into thermal calculation as a secondary heat source beside the arc heat. Generally the typical moment is chosen to be the moment when the arc is at the midpoint along the workpiece length, as shown in Figure 1.

Figure 2 shows the flowchart of the whole simulation procedure. The left part of the flowchart illustrates the coupling analysis. The coupling analysis approaches the multi-field interaction by iterative thermal and electromagnetic analyses. Firstly, a transient thermal analysis with only arc heat input is performed to provide initial temperature field. Then iterative analyses are performed with updated material properties until fulfilling the convergence criteria which is based on the temperature difference with the previous iteration step. The right part is the sequent thermo-mechanical analysis of multilayer deposition which calculates the temperature history and residual stress state in workpiece. Element birth and death (activation and deactivation) technique is used to simulate the additive process of material deposition.
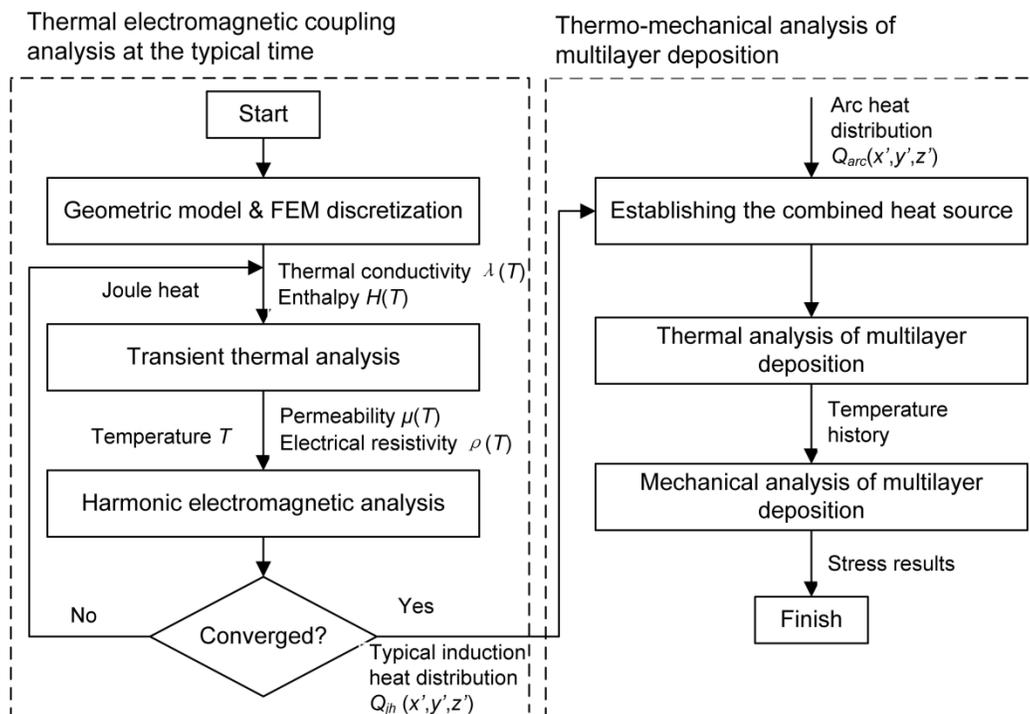

Figure 2: Flow chart of the simulation procedure

If both arc heat and induction heat distribution are indicated as functions of position in the moving arc coordinate (X',Y',Z'), then the combined heat source could be easily obtained by adding them up. The term "combined heat source" which represents the total energy input to workpiece from outside is introduced to facilitate discussions.

$$Q(x',y',z') = Q_{jh}(x',y',z') + Q_{arc}(x',y',z') \qquad (1)$$

The entire procedure is repeated to study on the two different ways of applying induction heat in WAM process, namely real-time preheating and postheating, in comparison with ordinary WAM process without

induction heating. The WAM process parameters are identical for the three cases. The induction system parameters are identical for both preheating and postheating except the position of inductor.

2. Numerical models

The 3D induction heating problem can be solved using the magnetic vector potential method that introduces magnetic vector potential A and electric scalar potential φ. The A-φ governing equations, as demonstrated by Biro and Preis [10], are derived from Maxwell's equations, Ohm's law and the electromagnetic constitutive relationships.

$$\nabla \times \frac{1}{\mu}(\nabla \times A) - \nabla \cdot \frac{1}{\mu}(\nabla \cdot A) + \sigma(\nabla \phi + \frac{\partial A}{\partial t}) - V \times \frac{1}{\mu}(\nabla \times A) = 0 \quad \text{in workpiece region} \quad (2)$$

$$\nabla \cdot (-\sigma \frac{\partial A}{\partial t} - \sigma \nabla \phi + V \times \frac{1}{\mu}(\nabla \times A)) = 0 \qquad \text{in workpiece region} \quad (3)$$

$$\nabla \times \frac{1}{\mu}(\nabla \times A) - \nabla \cdot \frac{1}{\mu}(\nabla \cdot A) = J_s \qquad \text{in air and coil region} \quad (4)$$

Using temperature-dependent electromagnetic properties of material is important for accurate solution. The electromagnetic properties of the used mild steel are shown in Figure 3.
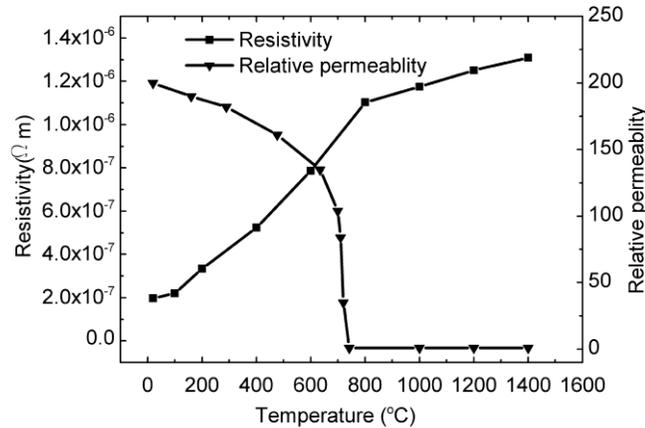

Figure 3: Electromagnetic properties varying with temperature

In the thermal analysis of WAM process, the formula used for arc heat is double ellipsoid heat source model [11] which describes arc heat mathematically in the moving arc coordinate (*X', Y', Z'*).

$$Q_{arc}(x', y', z') = \begin{cases} \dfrac{6\sqrt{3}f_r\eta UI}{a_r bc\pi\sqrt{\pi}} e^{\frac{-3x'^2}{a_r^2}} e^{\frac{-3y'^2}{b^2}} e^{\frac{-3z'^2}{c^2}} & x' < 0 \\ \dfrac{6\sqrt{3}f_f\eta UI}{a_f bc\pi\sqrt{\pi}} e^{\frac{-3x'^2}{a_f^2}} e^{\frac{-3y'^2}{b^2}} e^{\frac{-3z'^2}{c^2}} & x' \geq 0 \end{cases} \qquad (5)$$

$$f_r + f_f = 2 \qquad (6)$$

A combined radiation-convection heat transfer coefficient h is used in the prescribed thermal boundary condition on the workpiece surface [12].

$$\lambda \nabla T \cdot \hat{\boldsymbol{n}} + h(T - T_{amb}) = 0 \qquad (7)$$

$$h = \frac{\varepsilon \sigma_{sb}(T^4 - T_{amb}^4)}{(T - T_{amb})} + h_{con} \qquad (8)$$

where ε, σ_{sb}, h_{con}, T_{amb} are material emissivity, Stefan-Boltzmann constant, the convection coefficient and the ambient temperature, respectively.

In mechanical analysis, the kinematic hardening option, which uses the von Mises yield criteria coupled with a kinematic work hardening assumption, is applied as elastic-plastic material model. The structural restraints applied on FEM models are coincident with the real clamping conditions as shown in Figure 1 and the same for each simulation case.

All used thermal and mechanical properties of material are temperature-dependent. The latent heat generated by phase transformations is taken into account by modifying the specific heat curve with the change of temperature [13]. The thermal conductivities at temperatures above melt point are manually increased to 10 times the original value to imitate the convection effect due to the fluid flow in the weld pool [14]. The detailed data regarding the material properties of the used mild steel could be found in the references [4, 5, 15].

Results and discussion

1. Results of the thermo-electromagnetic coupling analysis

Identical deposition parameters are used in all the simulation cases, including wire feeding rate 3.6 m/min, arc power 6.36 kW and deposition speed 0.6 m/min, and the resulting component is 8mm thick and 1.5mm high per layer. The base plate is 72 mm high and 160mm long. The induction system parameters include coil current 600 A, frequency 250 kHz and inductor size $52 \times 18 \times 35$ mm.

For given inductor shape and current magnitude, the relative position of the inductor to the arc is the critical factor affecting the induction heat generation. The closer the inductor is to the arc, the less induction heat would be generated in workpiece, for the magnetic permeability and electrical conductivity of material decrease with increasing temperature. This inference is confirmed by the results of the coupling analysis as presented in Figure 5.

Figure 4 shows that, when the inductor is serving as real-time preheating ahead of the arc, the induction heat generation (Figure 4b) is negligibly affected by arc heat input; whereas arc heat causes a noticeable decrease of induction heat generation (Figure 4c) when the inductor is serving as real-time postheating behind the arc. The induction heat generated in and around high-temperature melt pool is so small that it can be ignored. Moreover, for both preheating and postheating, the induction heat concentrates on the edge of component, and the distributions resemble the coil in shape.

Further analyses that change the inductor position reveal the quantitative relationship between the distance D_x and the RMS Joule power P_{jh} in the whole workpiece. The result is shown in Figure 5. Positive value of D_x implies that the inductor is ahead of the arc torch. P_{jh} is much higher in preheating case than in postheating case. P_{jh} reaches its maximum and remain unchanged when D_x increases to about 32mm. P_{jh} has its minimum at the D_x of about -36mm when induction zone lies in hot region.
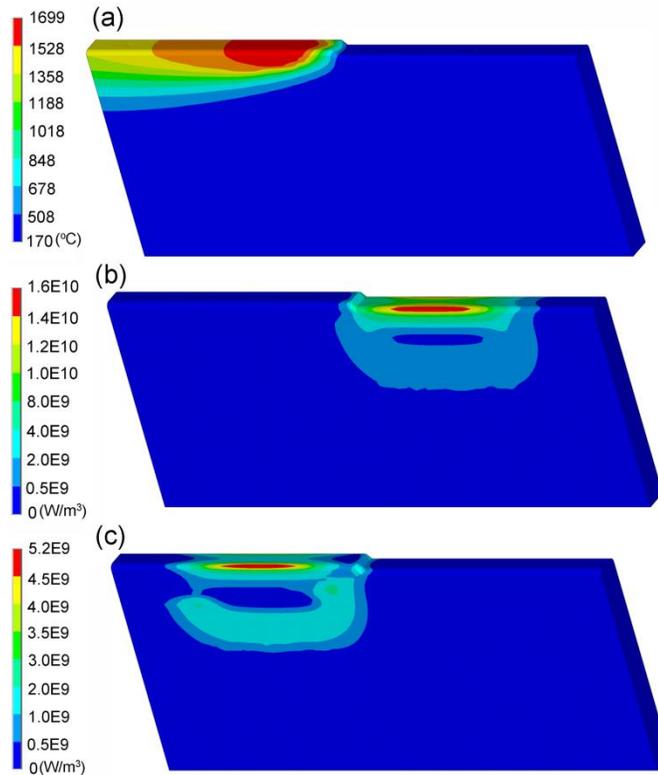
Figure4: The results of coupling analysis. (a) Initial temperature field for iterative calculation. Distributions of induction heat generation in the cases of (b) induction preheating, D_x =32mm, D_y =6mm, D_z =9mm and (c) induction postheating, D_x=-32mm, D_y=6mm, D_z=-9mm
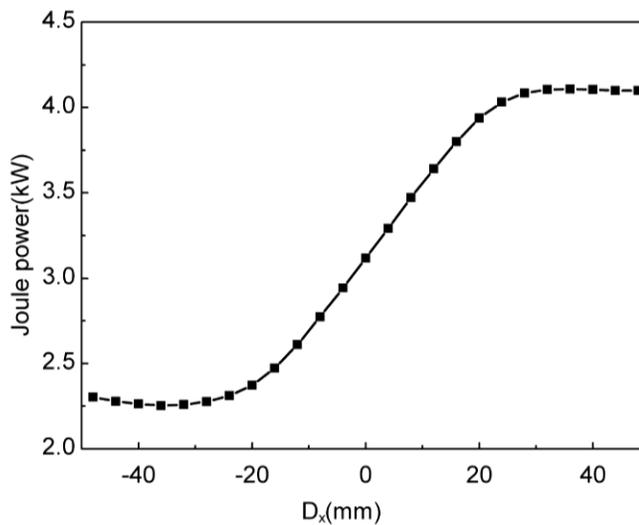

Figure 5: RMS Joule power varying with D_x

2. Results of the thermo-mechanical simulations for 2-layer deposition

Figure 6 exhibits the heat sources applied to thermal analysis of 2-layer WAM with different induction heating. The combined heat sources in both real-time induction preheating and postheating cases produce apparently stronger heat and larger heating zone than arc-only heat source.
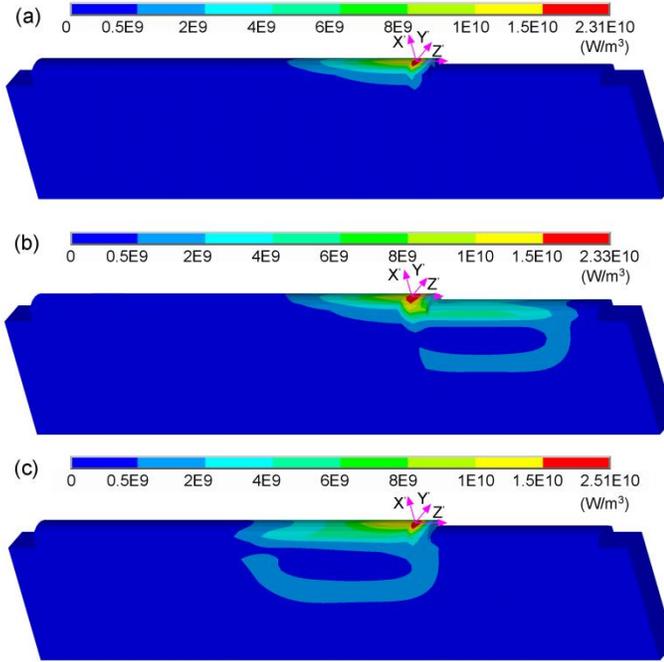
Figure 6: Heat sources applied to thermal analysis of 2-layer WAM processes with (a) no induction heating, (b) induction preheating and (c) induction postheating

As the combined heat source entirely passes by a specific position, the cumulative heat transferred to the material at this position might as well be denoted by the sign Q_{cum} with the unit J/m^3. Q_{cum} is a function of Y and Z coordinate; its distribution could be exhibited on the YZ cross-section of workpiece, as shown in Figure 7. Double ellipsoid heat source of arc yields a semi-elliptic Q_{cum} distribution with high gradients, whereas the gradients of Q_{cum} decrease when induction heat is combined, especially in Y direction. This is attributed to the mutual supplement of arc heat and induction heat as the former is strong in center region and the later is strong on surface due to skin effect.
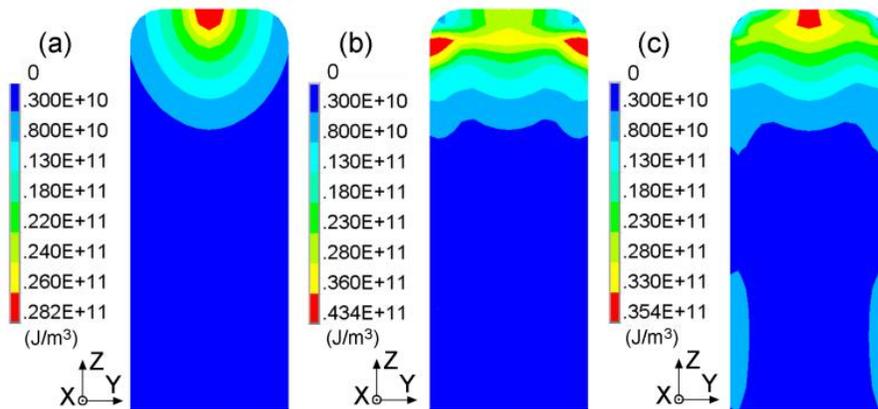

Figure 7: The distributions of the cumulative heat input Q_{cum} in AM processes with (a) no induction heating, (b) induction preheating and (c) induction postheating

The evolutions of temperature field during 2-layer deposition in each case are obtained by thermal analysis with different combined heat sources. To draw comparison more quantitatively, thermal cycle results at

a specific point P under different induction heating conditions are extracted and shown in Figure 8. It is obvious that material experiences the highest peak temperature in the case of induction preheating.
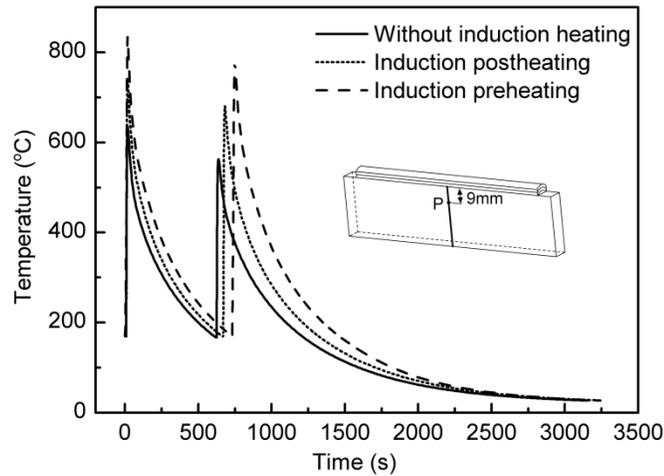

Figure 8: Thermal cycles at a specific position

Although the introduction of induction heat increases the total amount of heat input, the distribution of heat input has become more homogeneous in both time and space. This could be verified by the significant decrease of temperature gradients as shown in Figure 9. Figure 9 demonstrates that the use of induction heating decreases the temperature gradient in most area. The maximum gradient occurs around the liquid-solid interface.
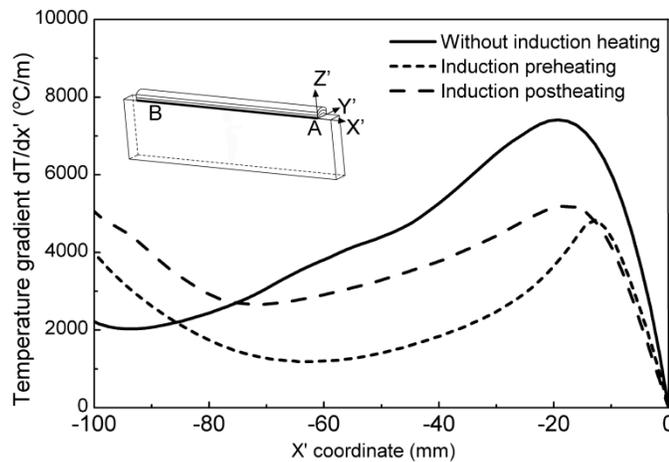

Figure 9: Temperature gradient dT/dx' along line AB when the arc center arrives at A from B for the first layer deposition

The von Mises stress distributions on the surface of workpiece when cooling to room temperature are shown in Figure 10. The high equivalent stress in red region indicates the material is approaching yield state. The red region becomes smaller when induction heating is employed for either preheating or postheating. And the induction preheating apparently produces the lowest residual stresses.
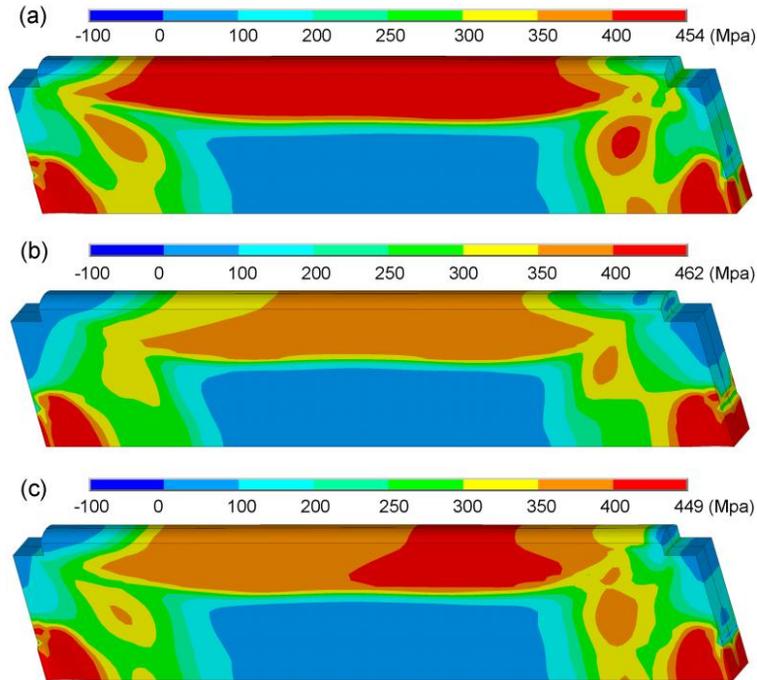
Figure 10: Equivalent von Mises stress when workpieces cool to room temperature after 2-layer deposition with (a) no induction heating, (b) induction preheating and (c) induction postheating

As tensile residual stress σ_x is probably of the most fundamental interest, σ_x on the surface of workpiece are measured using XRD method in order to validate the calculated results. Figure 11 exhibits the measured and the calculated σ_x along the central line CD. The experimental measurement qualitatively validates the stress reducing effect of induction preheating and postheating, though relatively large deviations are found between the calculated and the measured results. The deviations are chiefly caused by the measuring errors and the stress relief effect of removing clamping for measurement.
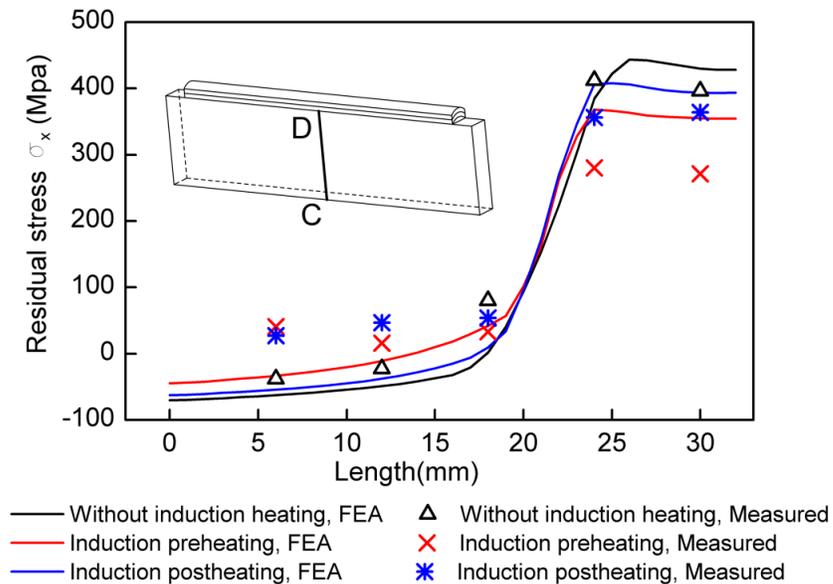

Figure 11: First principal stresses along central line CD

During WAM process, metallic materials are melted and deposited on the base plate which acts as a heat sink and mechanical constraint. The tensile stresses are generated when the thermal contraction of the heated volume is impeded during cooling by cooler volumes below. Metallic volumes shrink thermally according to their coefficient of thermal expansion and existing temperature difference. So the final residual stress is certainly dependent on thermal gradient. Figure 7 and Figure 9 have shown that induction preheating and postheating result in more homogeneous heat input and smaller thermal gradients, which might in return leads to the decrease of strain mismatch. This is the first mechanism of reducing residual stress. The second mechanism is that preheating introduces prior volumetric expansion and reduces the effective yield stress in material. The second mechanism is the major cause of stress-reducing effect of preheating. The absence of the second mechanism may be the reason why induction postheating performs worse in reducing stress than preheating.

Conclusion

This paper develops finite element models and simulation strategies for the simulation of the induction-assisted WAM process. By above, conclusions can be drawn as follows.

The simulation of induction-assisted WAM process must calculate at a large number of time steps to approach the actual temperature history. However, performing thermo-electromagnetic motion coupling analysis at each time step is computationally prohibitive. The simulation strategy proposed in the study has successfully solved this problem by simplifying induction heat as moving constant heat source, which is defined on the induction heat distribution obtained through the coupling analysis at a typical moment. In this way, reasonable results have been obtained at an acceptable computational cost.

Furthermore, the thermo-mechanical analyses of multilayer depositions show that both real-time induction preheating and postheating lead to the reduction of residual stresses despite of the increased heat input, and the real-time induction preheating is better by contrast in reducing stress. The residual stress measurement by XRD method also qualitatively verified this conclusion.

Acknowledgement

References

[1] Radaj D, 1992, "Heat effects of welding: temperature field, residual stress, distortion," Springer Berlin, Berlin, pp.263-265.

[2] Brückner F, Lepski D, Beyer E, 2007, "Modeling the Influence of Process Parameters and Additional Heat Sources on Residual Stresses in Laser Cladding," Journal of Thermal Spray Technology 16 (3):355-373.

[3] Mughal MP, Fawad H, Mufti RA, 2006, "Three-dimensional finite-element modelling of deformation in weld-based rapid prototyping," Proceedings of the Institution of Mechanical Engineers Part C-Journal of Mechanical Engineering Science 220 (6):875-885.

[4] Zhao H, Zhang G, Yin Z, 2011, "A 3D dynamic analysis of thermal behavior during single-pass multi-layer weld-based rapid prototyping," Journal of Materials Processing Technology 211 (3):488-495.

[5] Zhao H, Zhang G, Yin Z, 2012, "Three-dimensional finite element analysis of thermal stress in single-pass multi-layer weld-based rapid prototyping," Journal of Materials Processing Technology 212 (1):276-285.

[6] Ding J, Colegrove P, Mehnen J, Ganguly S, Sequeira Almeida PM, Wang F, Williams S, 2011, "Thermo-mechanical analysis of Wire and Arc Additive Layer Manufacturing process on large multi-layer parts," Computational Materials Science 50(12):3315-3322.

[7] Ding J, Colegrove P, Mehnen J, Williams S, Wang F, Almeida PS, 2013, "A computationally efficient finite element model of wire and arc additive manufacture," International Journal of Advanced Manufacturing Technology 70(1-4):227-236.

[8] Bai X, Zhang H, Wang G, 2013, "Improving prediction accuracy of thermal analysis for weld-based additive manufacturing by calibrating input parameters using IR imaging," International Journal of Advanced Manufacturing Technology, 69(5-8):1087-1095.

[9] Guha P, Nabi Mu, 2012, "Optimal control of a nonlinear induction heating system using a proper orthogonal decomposition based reduced order model," Journal of Process Control 22 (9):1681-1687.

[10] Biro O, Preis K, 1989, "On the use of the magnetic vector potential in the finite-element analysis of three-dimensional eddy currents," IEEE Transactions on Magnetics 25 (4):3145-3159

[11] Goldak J, Chakravarti AP, Bibby M, 1984, "A new finite element model for welding heat sources," Metallurgical Transaction B 15B (2):6

[12] Abid M, Siddique M, 2005, "Numerical simulation to study the effect of tack welds and root gap on welding deformations and residual stresses of a pipe-flange joint," International Journal of Pressure Vessels and Piping 82 (11):860-871.

[13] Ferro P, Porzner H, Tiziani A, Bonollo F, 2006, "The influence of phase transformations on residual stresses induced by the welding process - 3D and 2D numerical models," Modelling and Simulation in Materials Science and Engineering 14 (2):117-136.

[14] Heinze C, Schwenk C, Rethmeier M, 2012, "Effect of heat source configuration on the result quality of numerical calculation of welding-induced distortion," Simulation Modelling Practice and Theory 20 (1):112-123.

[15] Gale WF, Totemeier TC, 2003, "Smithells metals reference book," Butterworth-Heinemann, Oxford, pp.14-27.